Original Article

Regeneration of partially decellularized tracheal scaffolds in a mouse model of orthotopic tracheal replacement

Journal of Tissue Engineering
Volume 12: 1–11

DOI: 10.1177/20417314211017417
journals.sagepub.com/home/tej
SAGE

Lumei Liu[1], Sayali Dharmadhikari[1,2], Kimberly M Shontz[1], Zheng Hong Tan[3], Barak M Spector[4], Brooke Stephens[3], Maxwell Bergman[4], Amy Manning[5], Kai Zhao[4], Susan D Reynolds[6], Christopher K Breuer[1,2] and Tendy Chiang[1,4,5]

Abstract

Decellularized tracheal scaffolds offer a potential solution for the repair of long-segment tracheal defects. However, complete decellularization of trachea is complicated by tracheal collapse. We created a partially decellularized tracheal scaffold (DTS) and characterized regeneration in a mouse model of tracheal transplantation. All cell populations except chondrocytes were eliminated from DTS. DTS maintained graft integrity as well as its predominant extracellular matrix (ECM) proteins. We then assessed the performance of DTS in vivo. Grafts formed a functional epithelium by study endpoint (28 days). While initial chondrocyte viability was low, this was found to improve *in vivo*. We then used atomic force microscopy to quantify micromechanical properties of DTS, demonstrating that orthotopic implantation and graft regeneration lead to the restoration of native tracheal rigidity. We conclude that DTS preserves the cartilage ECM, supports neo-epithelialization, endothelialization and chondrocyte viability, and can serve as a potential solution for long-segment tracheal defects.

Keywords

Partially decellularized tracheal scaffolds, orthotopic tracheal replacement, extracellular matrix, neo-epithelialization, chondrocyte viability

Date received: 8 March 2021; accepted: 26 April 2021

Introduction

Despite advances in open and endoscopic airway surgery, there remains no cure for long-segment tracheal defects. Such defects can arise from congenital anomalies or develop as a complication following malignancy, trauma, or infection.[1] When these defects involve more than a third of the pediatric trachea, they are not able to be repaired using current surgical techniques. While rare, long-segment tracheal defects typically result in high morbidity and can be fatal.

There is no autologous tissue that can be used for tracheal replacement; efforts to use flaps and grafts for tracheal replacement surgery remain heroic.[2,3] Strategies for tracheal replacement have turned to regenerative medicine with the goal of creating tissue that is similar to the host

[1]Center for Regenerative Medicine, Abigail Wexner Research Institute, Nationwide Children's Hospital, Columbus, OH, USA
[2]Department of Pediatric Surgery, Nationwide Children's Hospital, Columbus, OH, USA
[3]Collage of Medicine, The Ohio State University, Columbus, OH, USA
[4]Department of Otolaryngology–Head & Neck Surgery, The Ohio State University Medical Center, Columbus, OH, USA
[5]Department of Pediatric Otolaryngology, Nationwide Children's Hospital, Columbus, OH, USA
[6]Center for Perinatal Research, Abigail Wexner Research Institute, Nationwide Children's Hospital, Columbus, OH, USA

Corresponding author:
Tendy Chiang, Center for Regenerative Medicine, Abigail Wexner Research Institute, Nationwide Children's Hospital, 555 S. 18th Street, Columbus, OH 43205, USA.
Email: Tendy.Chiang@nationwidechildrens.org

and capable of renewal and repair.[4] Approaches for tissue engineered tracheal graft fabrication have included the modification of allograft tissue as well as synthetic and decellularized scaffolds.[5] Allograft outcomes have been limited due to graft immunogenicity and synthetic tracheal scaffolds have exhibited poor epithelialization and neovascularization.[6,7] Initially, decellularization was geared toward removal of all native cellular material, thus limiting immunogenicity while preserving a natural scaffold composed of extracellular matrix (ECM).[8,9] Decellularized trachea have exhibited regeneration in pre-clinical models, however their clinical applications have remained limited. Barriers of successful DTS creation have been associated with limited chondrocyte regeneration and disruption of graft mechanical properties resulting in collapse.[10–13]

Given the immunoprivileged nature of chondrocytes, complete decellularization of donor trachea may not be necessary for a suitable tracheal replacement.[14–17] Contemporary approaches have begun to assess the feasibility of partial decellularization approaches, removing immunogenic cell types and preserving immunoprivileged chondrocytes.[18,19] We have developed a mouse model of orthotopic tracheal replacement which permits the assessment of the tracheal replacements in vivo.[7,20] Using this model, we studied the impact of partial decellularization on graft matrisome composition, chondrocyte viability, micro-mechanical properties, and evaluated the regenerative capacity of partially decellularized tracheal scaffolds (DTS) in vivo.

Material and methods

Animal care and ethics statement

The Institutional Animal Care and Use Committee (IACUC) of the Abigail Wexner Research Institute at Nationwide Children's Hospital reviewed, approved, and monitored the protocol (AR15-00090) prepared for this study. Humane care was provided in accordance with standards published by the Public Health Service, National Institutes of Health (NIH, Bethesda, MD) in the publication entitled Care and Use of Laboratory Animals (2011), as well as regulations defined in the Animal Welfare Act by USDA.

Generation of tracheal scaffolds

Tracheal segments were harvested from 6 to 8-week-old female C57BL/6 mice and trimmed to create grafts designed to approximate long-segment defects (3~4 mm length). Syngeneic tracheal grafts (STG) were harvested from donors and maintained in PBS at room temperature while the recipient animal was prepared for implant. Decellularized tracheal scaffolds (DTS) were fabricated as a modification of previously published methods.[21] Briefly, tracheas were subjected to sequential treatment at room temperature with solutions of 1% penicillin/streptomycin in PBS (rinse), 0.01% sodium dodecyl sulfate (SDS, 5 min), 0.9% NaCl solution (10, 15, and 20 min), 0.01% SDS (24 h), 0.1% SDS (24 h), 0.2% SDS (3 h), 0.1% SDS (3 h), 1% TritonX-100 (30 min). Tracheas were equilibrated in 0.9% NaCl solution overnight at 4°C. All decellularization steps occurred with agitation (48-rpm). Grafts were created in separate cohorts and reproducibility was validated prior to implantation. DTS were stored in PBS at –20°C prior to implantation. Axial and longitudinal images of native and DTS were used to assess gross morphology.

Mass spectrometry

We assessed the matrisome of native trachea and DTS with mass spectrometry.[22,23] Briefly, samples were digested by adding 5% SDS solution in 50mM Triethylammonium bicarbonate (TEAB) solution and lysed with probe and bioruptor sonicators. Protein concentration was measured using Qubit (Thermo Fisher Scientific). A total of 20 µg of protein from each sample were digested using S-Trap™ sample processing technology (Protifi, Farmington, NY, USA). A total of 1 ug of protein underwent liquid chromatography followed by tandem mass spectrometry (LC–MS/MS). The data were analyzed using MASCOT via Proteome Discoverer™ (Thermo Fisher Scientific, Waltham, MA, USA) and then summarized using Scaffold (Proteome Software, Inc., Portland, OR, USA). Spectral count was used as a semiquantitative measure of protein abundance.

DNA quantification

Extent of decellularization in DTS was quantified using a DNA extraction assay (DNeasy Blood & Tissue Kit, QIAGEN, MI) according to kit instructions.[24] Briefly, tracheas ($N=4$) were harvested and separated into proximal and distal grafts. Proximal grafts were decellularized for graft fabrication, and corresponding distal segments served as unoperated controls. Samples were weighed after blotting to remove excess moisture from the sample.[25–27]. Tissue was digested in 180 µl ATL and 20 µl proteinase K at 56°C overnight in capped tubes. Buffer AL (200 µl) and ethanol were added, and tubes were vortexed. The lysate was transferred to a DNeasy Mini spin column in a 2 ml collection tube and centrifuged at 8000 rpm for 1 min. The DNA retained in the spin column was washed with 500 µl Buffers AW1 and AW2 by centrifugation at 8000 rpm (1 min) and 14,000 rpm (3 min), respectively. DNA was eluted from the spin column by two washes of 200 µl AE buffer at 8000 rpm spinning for 1 min. DNA concentration (ng/mg wet tissue) was measured using the Nanodrop™ 2000c spectrophotometer (Thermo Fisher Scientific).

Scanning electron microscopy

Tracheal grafts were fixed in 2.5% glutaraldehyde (Sigma–Aldrich, St. Louis, MO, USA) in PBS (Gibco, Thermo Fisher Scientific) for 1 h at room temperature, then rinsed three times with PBS. Samples were lyophilized overnight, sputter-coated with gold-palladium, and imaged using scanning electron microscopy (SEM, SU4800, Hitachi, Japan).

Tracheal graft implantation

Segmental tracheal replacement was performed in C57BL/6 mice using STG ($N=8$) and DTS ($N=12$).[7] Briefly, upon anesthesia and sedation of an animal, a midline incision was made from the sternum to the hyoid bone in an aseptic fashion. The strap muscles were separated, and the trachea was dissected from the recurrent laryngeal nerves and esophagus. After the trachea was circumferentially dissected, it was transected below the third tracheal ring. The distal tracheal segment was sutured to the sternal notch, serving as a temporary tracheostomy site. The experimental graft (STG or DTS) was then sutured to the proximal airway using 9–0 sterile nylon suture in an interrupted fashion. The tracheostomy site was released and a 3~4 mm (three rings) segment of native trachea was excised. The distal graft was then sutured to the distal airway. A subset of STG and DTS recipients were implanted with radio-opaque markers at the proximal and distal anastomoses for micro-computed tomography (microCT). Animals were monitored and euthanized if humane endpoint criteria were met (respiratory distress, loss of >20% preimplantation weight). All surviving animals were euthanized at 28 days post-implantation and grafts were harvested. The tissues were formalin-fixed and embedded in paraffin for sectioning for downstream histology and immunofluorescent staining.

Micro-computed tomography

Graft patency was assessed in vivo with the Trifoil eXplore Locus RS 80 micro-computed tomography (microCT).[6] Live animal scanning was performed on post-operative day (POD) 0; animals were positioned prone following induction of inhalational anesthesia (1%−3% isoflurane in room air at 1–3 L/min). Terminal scans were performed at humane and experimental endpoints with similar positioning. Three-dimensional images of the airway lumen were reconstructed using Amira (Thermo Fisher Scientific).

Histology

Grafts were sectioned in both axial and longitudinal orientations for pre-implant characterization and in the longitudinal plane following explant to assess the host-graft interface.[7] Grafts ($N=13$) were randomly selected from three separate decellularization cohorts and stained with Masson's Trichrome, Alcian Blue, and Hematoxylin and Eosin (H&E) (Sigma–Aldrich, St. Louis, MO, USA) to confirm reproducibility of the protocol. Longitudinal sections of explanted tracheal grafts underwent immunofluorescence with quantification of epithelial and endothelial cells.[7] Epithelialization was measured as a function of % coverage of the graft with ciliated (ACT) and basal (K5, K14) cells. Restoration of the tracheal microvasculature was quantified by counting CD31+ cells per 20X field within the submucosa.

Chondrocyte viability was then assessed with both live / dead assay and terminal deoxynucleotidyl transferase dUTP nick end labeling (TUNEL) assay. Live/dead cytotoxicity kit (Invitrogen™, Thermofisher Scientific) was used to stain an isolated tracheal cartilage of STG and DTS with 0.6 µl/ml Calcein-AM and 13 µl/ml ethidium homodimer-1 in PBS (300 µl/sample). Following a 15-min incubation, transverse sections of the cartilage were imaged with a confocal microscope (Zeiss LSM700). Live cells were defined as green-fluorescent calcein-AM to indicate intracellular esterase activity and dead cells were defined as red-fluorescent ethidium homodimer-1 to indicate loss of plasma membrane integrity. Viability was quantified as percentage of living cells [Live $\%=100 \times (N_{\text{live cells}} / N_{\text{total cells}})\ \%$]. Apoptotic chondrocytes were quantified using the TUNEL assay (Sigma-Aldrich); chondrocytes were stained with Sox9 antibodies (primary: rabbit polyclonal antibody (1:400, Sigma-Aldrich), secondary: goat-anti-mouse Alexa Fluor 488 (1:500, Invitrogen, CA, USA)) with 1 µg/ml 4,6-diamidino-2-phenylindole (DAPI, Invitrogen) counterstain. Viability was derived by [Live $\%=100\times(N_{\text{nuclei}}+_{\text{sox9}}+_{\text{TUNEL}}- / N_{\text{nuclei}}+)\ \%$].

Atomic force microscopy

Regional micromechanics of grafts were measured using atomic force microscopy (AFM).[28–30] Tissue sections were de-paraffinized with xylene washes and rehydrated through graded alcohols, followed by overnight immersion in PBS at room temperature. Micromechanical properties of tissue samples were characterized using the Asylum MFP-3D-Infinity-BIO AFM.[31,32] In brief, a dull-tipped triangular probe (PNP-TR-Au, Asylum Research) with a nominal spring constant of ~0.32 N/m was used. The AFM system was calibrated following the manufacturer's instruction before each indentation measurement. Deflection inverse optical lever sensitivity was calculated from single force-generated curve and adjusted by re-installation of the cantilever when it was over 100 nm/V. The cantilever spring constant was confirmed using the thermal fluctuation method. Force-indentation profiles were acquired at a force distance of 1.6 µm, scan rate of 0.3 Hz and sample rate 625 Hz.

Tracheal sections ($N=3$/group) from native, DTS, STG (28d) and DTS (28d) were quantified. For each animal, continuous force (40 curves/point) was used to test six locations in epithelium and submucosa of the native trachea and grafts recovered at 28-day timepoints. Due to the lack of epithelial cells in DTS prior to implantation, only three locations were tested in epithelium and submucosa. In cartilage, continuous force was used to test chondrocytes, perichondrium, and extracellular matrix (ECM) locations (six sites for chondrocytes, three for perichondrium and four for ECM per sample). Samples were immersed in PBS while testing under a "Bio-contact cell" mode. The trigger points for all regions were 1V~2V. The Young's modulus of each point was determined by fitting force-indentation data from 40 curves to the Oliver-Pharr model (a modified Hertz model) using IGOR Pro software (WaveMetrics).[28,33]

Statistical analysis

Statistical analysis was performed using the GraphPad Prism 8 software (GraphPad Software Inc., CA, USA). The normality of data was evaluated using Shapiro-Wilk test. Normally-distributed data were compared using Welch's *t*-test for data with non-equal variances and unpaired *t*-test for data with equal variances. Non-parametric test (Mann–Whitney) was used for non-normally distributed data. Statistical difference was considered significant at $p<0.05$. All experimental data were expressed as mean ± standard deviation (SD).

Results

Decellularization eliminated cells within the epithelium while preserving chondrocytes and extracellular matrisome

We first created DTS that were grossly similar to native trachea (Figure 1(a)). Axial inspection confirmed that the graft lumen remained patent. Partial decellularization was confirmed with DNA assay, demonstrating a 51.58 % reduction in DNA content (Figure 1(b), $p=0.0090$). The tracheal lumen was inspected with scanning electron microscopy, qualitatively demonstrating decellularization of the epithelium in the DTS, revealing the underlying ECM fibers, and devoid of the cells seen in the native epithelium (Figure 1(c)). Light microscopy imaging revealed that graft decellularization was reproducible, consistently limited to the epithelium and epithelial submucosa (Figure 1(d), longitudinal images not shown). The tracheal cartilage of DTS was histologically identical to control: chondrocytes remained nucleated and the staining intensities of the extracellular matrix (ECM) proteins, collagen (Masson's Trichrome) and glycosaminoglycans (GAGs, Alcian blue) were similar to native tracheal sections (Figure 1(d)). We then examined the impact of decellularization on key matrix proteins of the trachea with mass spectrometry. Spectral count of graft proteins showed that partial decellularization did not result in the loss of graft collagen, GAGs, laminin, and fibronectin (Figure 1(e)).

Orthotopic implant of the graft was performed to repair a segmental defect created in the native trachea (Figure 2(a-1)). Micro-computed tomography (microCT) following implantation confirmed post-implantation graft patency (Figure 2(a-2). Three-dimensional tracheal airway reconstructed from microCT scans reveal that grafts at endpoint (28 days) remained patent without evidence of graft stenosis or collapse (Figure 2(b)).

Decellularized tracheal scaffolds supported graft epithelialization, vascularization, and chondrocyte viability in vivo

We performed orthotopic segmental tracheal replacement in mice using DTS and STG (control). Survival to the planned euthanasia timepoint of STG recipients was 87.50% (7/8), compared to 41.67% of DTS recipients (5/12, $p=0.0490$, Log-rank (Mantel–Cox) test). Most animals requiring early euthanasia ($N=7$) exhibited signs of respiratory distress within the first week after surgery. One animal was found dead at day 20. No animals at the experimental endpoint exhibited signs of respiratory distress. Immunofluorescence confirmed the elimination of graft epithelial cells in DTS prior to implantation (Figure 3(a–c)). We found that DTS support basal cell (BC) coverage in vivo (K5+ = 95.95 ± 2.17%) at endpoint, equivalent to native trachea (Figure 3(a)). Compared to STG, BC K14+ expression was higher in DTS (Figure 3(b)), consistent with BC activation during injury and repair.[34] In Figure 3(c), ciliated epithelial cells were also found to be lining the lumen of DTS at 28 days (63.33 ± 14.12%), albeit less than syngeneic controls (87.13 ± 4.59%, $p=0.0173$) and adjacent native trachea (90.02 ± 5.26%, $p=0.0104$). Decellularization also resulted in the successful elimination of the endothelial cells of the tracheal epithelial microvasculature ($p=0.0050$, Figure 3(d)). In vivo implantation of DTS resulted in the restoration of tracheal endothelial cells; CD31+ cells were equivalent to native and STG at endpoint ($p=0.6254$ and 0.8333, respectively).

To further assess the effect of partial decellularization on the graft cartilage, we quantified chondrocyte viability using live / dead assay (Figure 4(a)) and TUNEL assay (Figure 4(b)). Both native and STG exhibited high chondrocyte viability which persisted following orthotopic implantation in vivo. Viability of chondrocytes in DTS at the time of implantation was low (2.00 ± 3.46% via live/dead and 4.30 ± 3.89% via TUNEL), however this increased following orthotopic implantation (live / dead – 25.97 ± 10.99%, $p=0.0187$ and TUNEL – 18.58 ± 4.42%, $p=0.0208$).

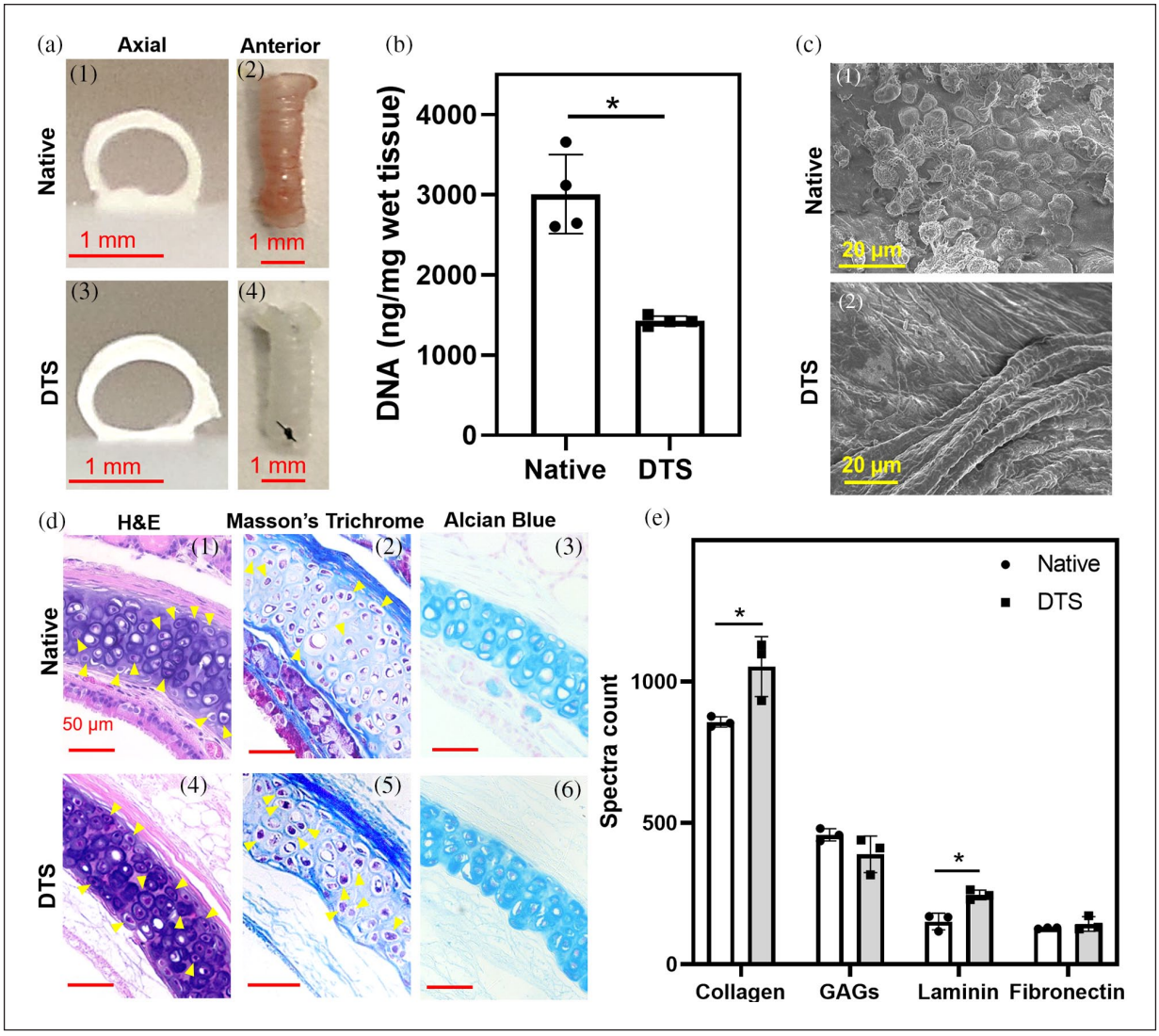

Figure 1. Characterization of decellularized tracheal scaffold (DTS): (a) gross axial and anterior images of native trachea ((1), (2)) and DTS ((3), (4)), (b) DNA quantification (ng/mg wet tissue); * represents a loss of DNA following decellularization ($p = 0.0090$), (c) representative SEM images of native trachea (1) and DTS (2), (d) representative axial H&E, Masson's Trichrome and Alcian blue stained sections for native trachea (1–3) and DTS (4–6). Solid arrows denote representative chondrocytes in H&E and Masson's Trichrome images, and (e) spectral count of collagen, glycosaminoglycans (GAGs), laminin and fibronectin; * denotes a difference between native and DTS in collagen and laminin ($p = 0.0342$ and 0.0149, respectively).

Decellularized tracheal scaffolds restored native micromechanical properties in vivo

We then assessed the micromechanical properties of DTS during graft regeneration, quantifying the impact of decellularization and implantation on the Young's modulus of various regions of the trachea: epithelium and submucosa, and cartilage (perichondrium, chondrocytes, and cartilage ECM). We confirmed that decellularization resulted in a loss of stiffness within the previously-cellularized regions of the trachea (epithelial region: 44.06% decrease, $p = 0.0259$; chondrocytes: 52.94% decrease, $p = 0.0016$), while preserving the stiffness of the ECM and perichondrium (Figure 5). Following implant, regional stiffness of the epithelium and submucosa was equivalent to STG, suggesting that graft regeneration restored native graft stiffness ($p = 0.8931$). Using a similar rationale, we found that the loss of stiffness seen in the chondrocytes of DTS at the time of implant was restored to normal conditions after implantation, suggesting chondrocyte recovery.

Discussion

We present an approach to tracheal replacement using partially decellularized tracheal scaffolds (DTS). We successfully created a graft that removed the donor epithelial cells

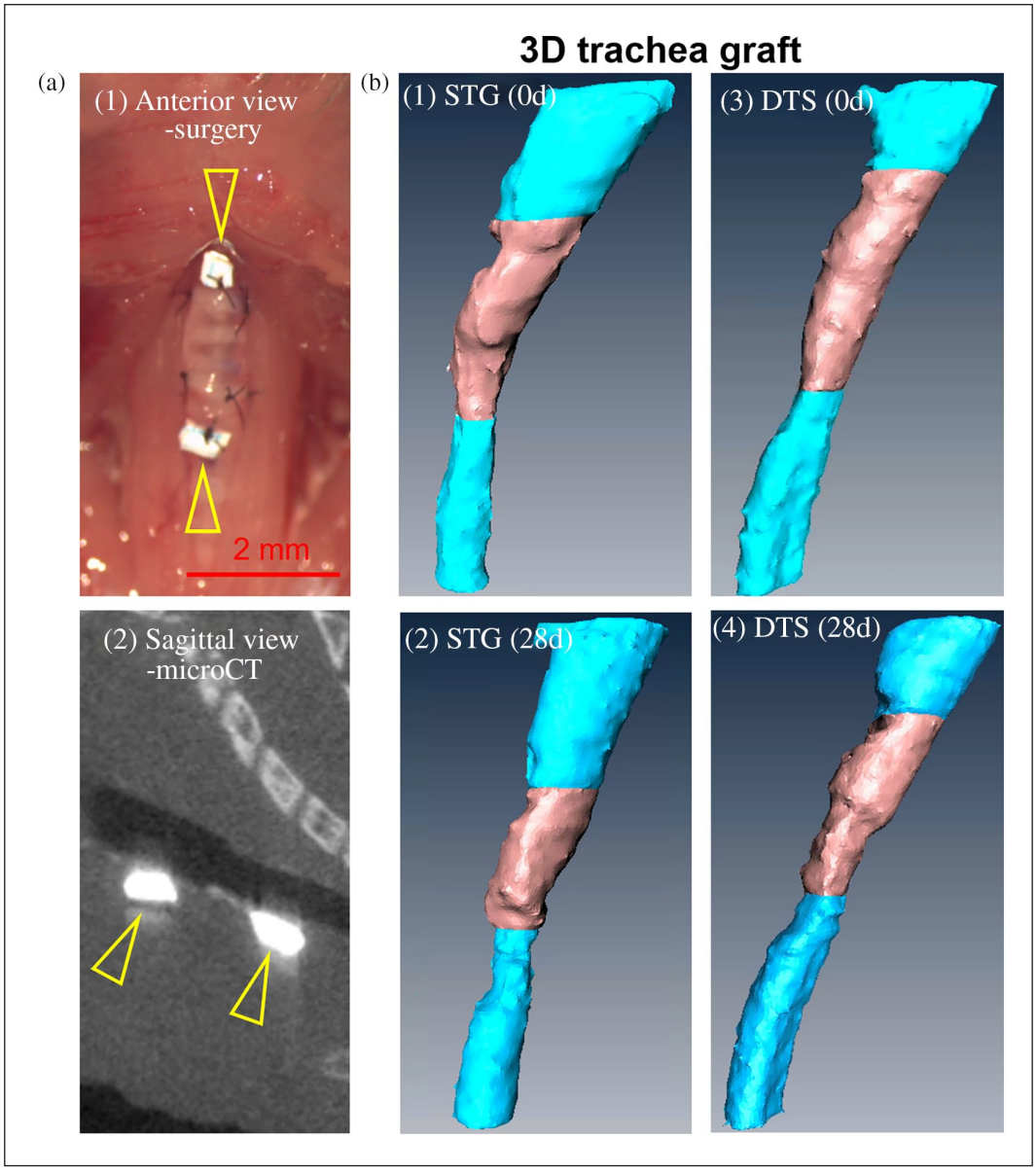

Figure 2. Graft implantation and microCT characterization: (a) representative images of DTS post-implantation (1) anterior image of implanted graft in vivo, (2) sagittal microCT image of implanted graft (open arrows – radio-opaque markers) and (b) three-dimensional reconstructions of STG (1), (2) and DTS (3), (4) at day 0 and 28 in vivo.

and preserved chondrocytes in the tracheal cartilage. Unlike previous approaches of complete decellularization, our goals for partial decellularization included: (1) complete removal of cells within the surface airway epithelium, epithelial submucosa, and microvasculature; (2) preservation of the basement membrane and ECM of the epithelial submucosa; (3) preservation of cartilaginous ECM and minimizing exposure of graft chondrocytes to decellularization detergents.

As decellularization can cause ECM injury resulting in disruptions in graft biomechanics, we assessed the effect of partial decellularization on DTS by quantifying the graft matrisome as well as its regional micromechanical properties prior to implantation.[35,36] We identified that DTS fabrication resulted in preservation of key ECM proteins essential for biomechanical support and maintained consistent micromechanical properties in the matrix.[37] A key advantage of partial decellularization in our DTS was its ability to preserve cartilage integrity. As such, we used atomic force microscopy (AFM) to further characterize chondrocyte stiffness in addition to live / dead and TUNEL assays. AFM offers superior resolution to optical microscopy to assess cell properties: loss of cell stiffness can suggest membrane injury;[22,38] the reduction of cellular rigidity can indicate the damage and destruction of cytoskeleton;[39] decreased cell stiffness can reveal cell apoptosis.[40]

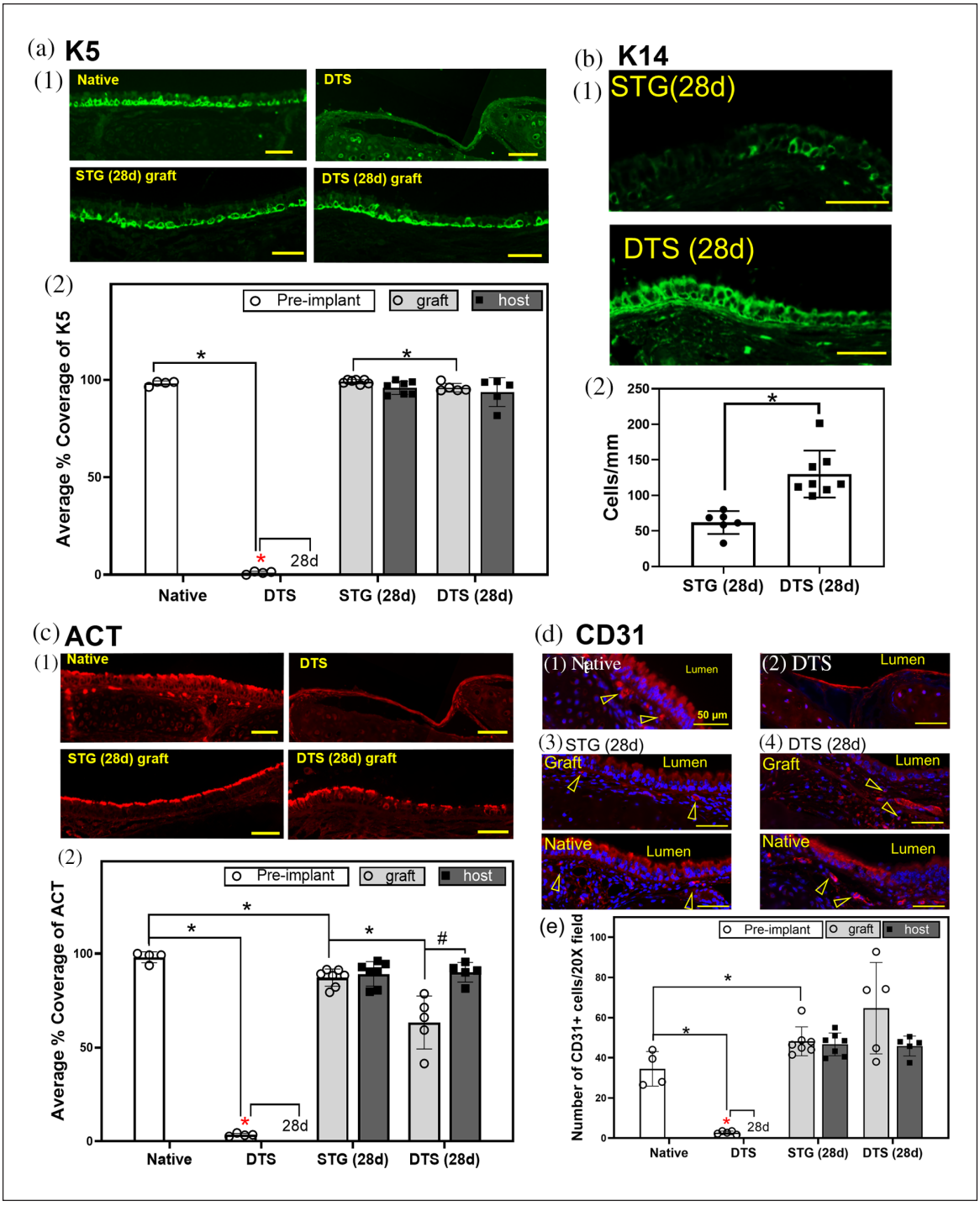

Figure 3. Decellularized tracheal scaffolds following orthotopic implantation: (a) basal cells (K5+) on STG and DTS (1) representative images; (2) quantification of K5+ basal cell coverage on graft (average % coverage of K5); * represent difference between native vs DTS, STG (28 d) graft vs DTS (28 d) graft, and DTS vs all 28 d basal cell coverage ($p < 0.05$), (b) K14+ basal cells in STG and DTS: (1) representative images; (2) quantification of K14+ cell coverage (cells/mm); * denote increase in K14+ basal cells on DTS graft at day 28 ($p = 0.0007$) compared to STG, (c) quantification of ciliated epithelial cells (ACT+) in STG and DTS prior implantation and at day 28: (1) representative images; (2) quantification of K5+ basal cell coverage on graft (average % coverage of ACT); * difference between native vs DTS, native vs STG (28 d) graft, STG (28 d) graft vs DTS (28 d) graft, and DTS vs all 28 d basal cell coverage ($p < 0.05$); # denote difference between DTS (28 d) graft vs DTS (28 d) native ($p < 0.05$), and (d) characterization of endothelial cells (CD31+) in STG and DTS: (1) representative images, empty arrow heads denote CD31+ cells; (2) quantification of CD31+ cells within the tracheal microvasculature (number/20X image); * represent difference between compared groups.

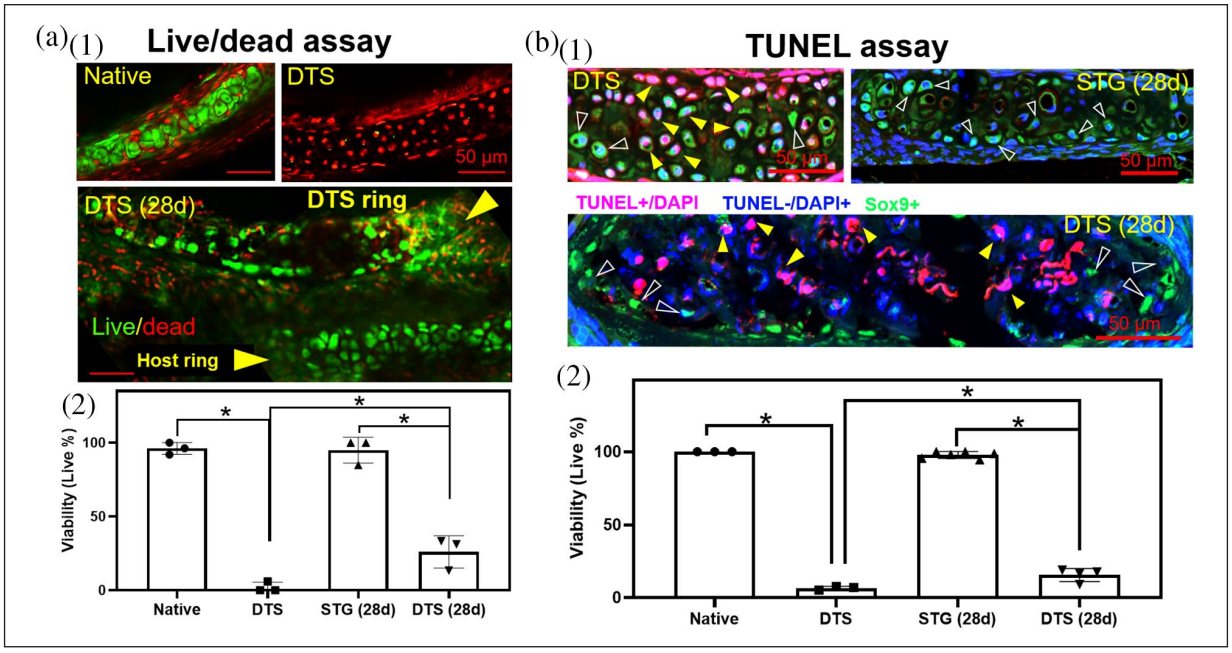

Figure 4. Chondrocyte viability characterization: (a) live/dead assay (1 and 2); arrow heads point out a DTS ring and a host ring; * represent lower viability of DTS comparing with native and DTS (28 d) ($p < 0.0001$, and 0.0187, respectively), and lower viability of DTS (28 d) comparing with STG (28 d) ($p < 0.0001$) and (b) TUNEL assay (1 and 2); empty arrow heads point representative live cells (TUNEL-DAPI+Sox9+, blue nuclei and green cytoplasm) in TUNEL assay, and solid arrow heads point out representative apoptotic cells (TUNEL+DAPI+, purple nuclei) in TUNEL assay; * denote lower viability of DTS comparing with native and DTS (28 d) ($p < 0.0001$ and 0.0208, respectively), and lower viability of DTS (28 d) comparing with STG (28 d) ($p < 0.0001$).

Decellularization resulted in a loss of stiffness in epithelial regions (epithelial and epithelial submucosa) and these micromechanical properties were restored following graft regeneration at 28 days. Similarly, a loss of stiffness was noted in graft chondrocytes after decellularization; however, this was restored at 28 days in vivo equivalent to native and syngeneic cohorts.

We found that DTS supported epithelial coverage in vivo with observation of basal and ciliated epithelial subtypes, confirming that partially-decellularized scaffolds can support epithelial regeneration. In addition, we found that DTS were able to repopulate CD31+ endothelial cells within the graft submucosa comparable to that of adjacent host tissue and syngeneic grafts. Further work will be devoted to assessing graft perfusion and microvascular function within DTS.

Our study has several limitations. First, despite the histologic preservation of graft chondrocytes, overall chondrocyte viability remained poor. We were able to increase viable chondrocytes within DTS in vivo in 28 days. Chondrocyte viability plays a critical role in maintaining the biochemical and biomechanical properties necessary to prevent stenosis or collapse in tracheal replacement, however the preservation of chondrocyte viability remains a challenge in tracheal tissue engineering.[19,41,42] Modulation of decellularization protocol, such as optimization of decellularization time, can preserve viability of chondrocytes in DTS.[19]

We also observed a higher mortality rate of hosts receiving DTS than that of STG control (p = 0.0490). A robust assessment of survival benefit is not permitted given the limited sample size. In addition, given the technical challenges of orthotopic tracheal replacement in a mouse model, it is difficult to associate survival outcomes exclusively with graft performance. As expected, animals that required early euthanasia exhibited less epithelialization than animals that met endpoint, however the presence of signs of graft dysfunction requiring early euthanasia and disparities in time points do not permit comparison of these groups (data not shown). In our analysis, we placed an emphasis on the characterization of asymptomatic hosts of each graft type at the experimental endpoint. Future efforts will be devoted to both defining the mode of failure in animals that required early euthanasia, as well as develop strategies to optimize graft performance in the early phases of repair.

Conclusion

Partially-decellularized tracheal scaffolds are a potential solution to repair long segmental tracheal defects. An approach that can completely eliminate cells in epithelium, epithelial submucosa, and microvasculature, while preserving critical structures to promote regeneration, including the basement membrane, ECM of the epithelial submucosa and cartilage,

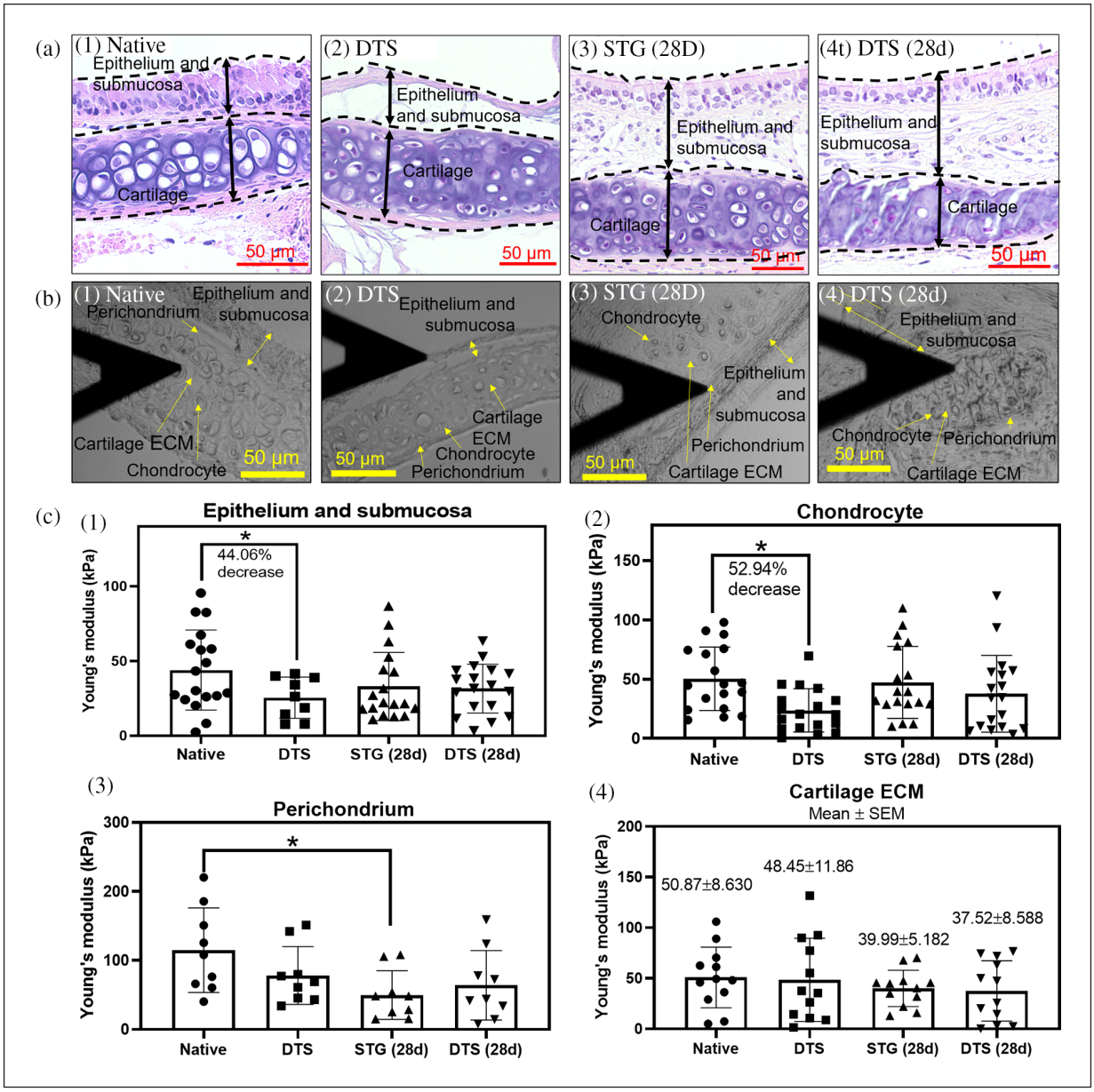

Figure 5. Micromechanics of tracheal grafts: (a) representative boundaries of regions tested in (1) native trachea, (2) DTS, (3) STG (28 d), and (4) DTS (28 d), (b) tissue sections of (1) native trachea, (2) DTS, (3) STG (28 d), and (4) DTS (28 d) with the AFM cantilever, and (c) Young's modulus of (1) epithelium and submucosa, (2) chondrocytes, (3) perichondrium, and (4) cartilaginous ECM. * denote differences in local stiffness between native and DTS in region of epithelium and submucosa, and chondrocyte ($p = 0.0295$ and 0.0016 respectively). * also denote difference between native and STG (28 d) in perichondrium ($p = 0.0140$).

and viable chondrocytes, may provide a supportive, non-immunogenic scaffold for host-derived tracheal regeneration.

Declaration of conflicting interests

The author(s) declared no potential conflicts of interest with respect to the research, authorship, and/or publication of this article.

Funding

The author(s) disclosed receipt of the following financial support for the research, authorship, and/or publication of this article: The authors acknowledge technical support from animal care and veterinary staff and the Morphology Core, and Terri Shaffer from the Small Animal Imaging Facility (SAIF) at the Abigail Wexner Research Institute at Nationwide Children's Hospital. The authors also thank Dr. Liwen Zhang at the Campus Chemical Instrument Center, Ohio State University for technical support of mass spectrometry analysis (supported by CCTS voucher award #5955, the CTSA Grant #UL1TR002733). Atomic Force Microscope in this study was supported by the National Institute of Health (S10 OD023438, Aaron J. Trask is the recipient). We also acknowledge Dr. Aaron J. Trask and Dr. Patricia McCallinhart for

sharing AFM equipment and technical support. This work was supported by the National Institute of Health (NIH NHLBIK08HL, TC is the recipient).

ORCID iDs

Lumei Liu https://orcid.org/0000-0001-9849-6881

References

1. Grillo HC. *Surgery of the trachea and bronchi*. Lewiston, NY: BC Decker, 2004, pp.839–850.
2. Kolb F, Simon F, Gaudin R, et al. 4-Year follow-up in a child with a total autologous tracheal replacement. *N Engl J Med* 2018; 378: 1355–1357.
3. Martinod E, Chouahnia K, Radu DM, et al. Feasibility of bioengineered tracheal and bronchial reconstruction using stented aortic matrices. *JAMA* 2018; 319: 2212–2222.
4. Chiang T, Pepper V, Best C, et al. Clinical translation of tissue engineered trachea grafts. *Ann Otol Rhinol Laryngol* 2016; 125(11): 873–885.
5. Greaney AM and Niklason LE. The history of engineered tracheal replacements: interpreting the past and guiding the future. *Tissue Eng Part B Rev*. Epub ahead of print 9 November 2020. DOI: 10.1089/ten.TEB.2020.0238.
6. Dharmadhikari S, Best CA, King N, et al. Mouse model of tracheal replacement with electrospun nanofiber scaffolds. *Ann Otol Rhinol Laryngol* 2019; 128: 391–400.
7. Dharmadhikari S, Liu L, Shontz K, et al. Deconstructing tissue engineered trachea: Assessing the role of synthetic scaffolds, segmental replacement and cell seeding on graft performance. *Acta Biomater* 2020; 102: 181–191.
8. Gilpin A and Yang Y. Decellularization strategies for regenerative medicine: from processing techniques to applications. *BioMed Res Int* 2017; 2017: 9831534.
9. Porzionato A, Stocco E, Barbon S, et al. Tissue-engineered grafts from human decellularized extracellular matrices: a systematic review and future perspectives. *Int J Mol Sci* 2018; 19: 4117.
10. Elliott MJ, De Coppi P, Speggiorin S, et al. Stem-cell-based, tissue engineered tracheal replacement in a child: a 2-year follow-up study. *Lancet* 2012; 380: 994–1000.
11. Elliott MJ, Butler CR, Varanou-Jenkins A, et al. Tracheal replacement therapy with a stem cell-seeded graft: lessons from compassionate use application of a GMP-compliant tissue-engineered medicine. *Stem Cells Transl Med* 2017; 6: 1458–1464.
12. Hamilton NJ, Kanani M, Roebuck DJ, et al. Tissue-engineered tracheal replacement in a child: a 4-year follow-up study. *Am J Transplant* 2015; 15: 2750–2757.
13. Kutten JC, McGovern D, Hobson CM, et al. Decellularized tracheal extracellular matrix supports epithelial migration, differentiation, and function. *Tissue Eng Part A* 2015; 21: 75–84.
14. Liu Y, Nakamura T, Sekine T, et al. New type of tracheal bioartificial organ treated with detergent: maintaining cartilage viability is necessary for successful immunosuppressant free allotransplantation. *ASAIO J* 2002; 48: 21–25.
15. Tanaka H, Maeda K and Okita Y. Transplantation of the cryopreserved tracheal allograft in growing rabbits. *J Pediatr Surg* 2003; 38: 1707–1711.
16. Cleven HA, Genden EM and Moran TM. Reepithelialized orthotopic tracheal allografts expand memory cytotoxic T lymphocytes but show no evidence of chronic rejection. *Transplantation* 2005; 79: 861–868.
17. Genden EM, Iskander A, Bromberg JS, et al. The kinetics and pattern of tracheal allograft re-epithelialization. *Am J Respir Cell Mol Biol* 2003; 28: 673–681.
18. Cui P, Liu P, Li S, et al. De-epithelialized heterotopic tracheal allografts without immunosuppressants in dogs: long-term results for cartilage viability and structural integrity. *Ann Otol Rhinol Laryngol* 2020; 130(5): 441–449.
19. Aoki FG, Varma R, Marin-Araujo AE, et al. De-epithelialization of porcine tracheal allografts as an approach for tracheal tissue engineering. *Sci Rep* 2019; 9: 12034.
20. Wiet MG, Dharmadhikari S, White A, et al. Seeding and implantation of a biosynthetic tissue-engineered tracheal graft in a mouse model. *J Vis Exp* 2019; 146: 59173.
21. Batioglu-Karaaltin A, Ovali E, Karaaltin MV, et al. Decellularization of trachea with combined techniques for tissue-engineered trachea transplantation. *Clin Exp Otorhinolaryngol* 2019; 12: 86.
22. Wang J, Wan Z, Liu W, et al. Atomic force microscope study of tumor cell membranes following treatment with anti-cancer drugs. *Biosens Bioelectron* 2009; 25: 721–727.
23. Ryzhuk V, Zeng X, Wang X, et al. Human amnion extracellular matrix derived bioactive hydrogel for cell delivery and tissue engineering. *Mater Sci Eng C Mater Biol Appl* 2018; 85: 191.
24. Qiagen A. *DNeasy© blood and tissue handbook*. Hombrechtikon, Switzerland: Qiagen AG, 2006.
25. Den Hondt M, Vanaudenaerde B, Maughan E, et al. An optimized non-destructive protocol for testing mechanical properties in decellularized rabbit trachea. *Acta Biomater* 2017; 60: 291–301.
26. Butler CR, Hynds RE, Crowley C, et al. Vacuum-assisted decellularization: an accelerated protocol to generate tissue-engineered human tracheal scaffolds. *Biomaterials* 2017; 124: 95–105.
27. Xu Y, Li Y, Liu Y, et al. Surface modification of decellularized trachea matrix with collagen and laser micropore technique to promote cartilage regeneration. *Am J Transl Res* 2019; 11: 5390.
28. McCallinhart PE, Cho Y, Sun Z, et al. Reduced stiffness and augmented traction force in type 2 diabetic coronary microvascular smooth muscle. *Am J Physiol Heart Circ Physiol* 2020; 318: H1410–H1419.
29. Timashev P, Koroleva A, Konovalov N, et al. Atomic force microscopy of tissue sections is a useful complementary tool in biomedical morphological studies. *Современные технологии в медицине* 2018; 10: 70–80.
30. Sapi E, Balasubramanian K, Poruri A, et al. Evidence of in vivo existence of Borrelia biofilm in borrelial lymphocytomas. *Eur J Microbiol Immunol* 2016; 6: 9–24.

31. Liu F, Mih JD, Shea BS, et al. Feedback amplification of fibrosis through matrix stiffening and COX-2 suppression. *J Cell Biol* 2010; 190: 693–706.
32. Shkumatov A, Thompson M, Choi KM, et al. Matrix stiffness-modulated proliferation and secretory function of the airway smooth muscle cells. *Am J Physiol Lung Cell Mol Physiol* 2015; 308: L1125–L1135.
33. Akhtar R, Schwarzer N, Sherratt M, et al. Nanoindentation of histological specimens: mapping the elastic properties of soft tissues. *J Mater Res* 2009; 24: 638.
34. Ghosh M, Ahmad S, Jian A, et al. Human tracheobronchial basal cells. Normal versus remodeling/repairing phenotypes in vivo and in vitro. *Am J Respir Cell Mol Biol* 2013; 49: 1127–1134.
35. Yang Z, Shi Y, Wei X, et al. Fabrication and repair of cartilage defects with a novel acellular cartilage matrix scaffold. *Tissue Eng Part C Meth* 2010; 16: 865–876.
36. Zhao YH, Yang Q, Xia Q, et al. In vitro cartilage production using an extracellular matrix-derived scaffold and bone marrow-derived mesenchymal stem cells. *Chin Med J (Engl)* 2013; 126: 3130–3137.
37. Liu L, Stephens B, Bergman M, et al. Role of collagen in airway mechanics. *Bioengineering* 2021; 8: 13.
38. Nikolaev NI, Müller T, Williams DJ, et al. Changes in the stiffness of human mesenchymal stem cells with the progress of cell death as measured by atomic force microscopy. *J Biomech* 2014; 47: 625–630.
39. Cai X, Yang X, Cai J, et al. Atomic force microscope-related study membrane-associated cytotoxicity in human pterygium fibroblasts induced by mitomycin C. *J Phys Chem B* 2010; 114: 3833–3839.
40. Kim KS, Cho CH, Park EK, et al. AFM-detected apoptotic changes in morphology and biophysical property caused by paclitaxel in Ishikawa and HeLa cells. *PLoS One* 2012; 7: e30066.
41. Lu T, Huang Y, Qiao Y, et al. Evaluation of changes in cartilage viability in detergent-treated tracheal grafts for immunosuppressant-free allotransplantation in dogs. *Eur J Cardio Thoracic Surg* 2018; 53: 672–679.
42. Yue L, Vuong B, Yao H, et al. Doxycycline preserves chondrocyte viability and function in human and calf articular cartilage ex vivo. *Physiol Rep* 2020; 8: e14571.